Viscous-Force-Dominated Tensile Deformation Behavior of Oriented Polyethylene

Bing Na, Qin Zhang, and Qiang Fu*

Department of Polymer Science & Materials, Sichuan University, State Key Laboratory of Polymer Materials Engineering, Chengdu, 610065, P.R. China

Yongfeng Men

Changchun Institute of Applied Chemistry, Chinese Academy of Science, Changchun 130022, P.R. China

Ke Hong* and Gert Strobl

Physikalisches Institut, Albert-Ludwigs-Universität, Hermann-Herder-Str. 379104 Freiburg, Germany

Received November 22, 2005; Revised Manuscript Received February 7, 2006

ABSTRACT: High-density polyethylene with shish-kebab structure, prepared by a melt extrusion drawing, was employed to investigate the effect of the well-defined lamellar orientation on the deformation characteristics under uniaxial tensile deformation along the drawing direction. This was done by investigating the true stress−true strain dependencies at different strain rates, recovery properties, and stress relaxation measurements. Measurements were complemented by recording in-situ wide-angle X-ray scattering patterns during the deformation process. The oriented samples showed not only a higher modulus, but different from analogous isotropic samples, a homogeneous deformation without necking. The true strain associated with the onset of fibrillation was determined. Because of the preorientation, it is shifted to 0.3, which is below the value 0.6 of the isotropic counterpart. The main finding is a strong enhancement of the viscous force, as was revealed by stress relaxation experiments; the viscous force takes up 70% of the total stress. The presence of shish-kebabs, i.e., interconnected lamellae in a stack, seems to be responsible for the high viscous force in the oriented samples. The absence of necking has to be ascribed to the high viscous force. The viscous force, which increases with the strain, gives also a major contribution to the measured tensile modulus.

1. Introduction

Because of its theoretical and technical significance, the search for relationships between the molecular structure and mechanical properties of polyethylene has been extensively conducted in the past.[1−10] The two-phase structure leads to peculiarities in the structure evolution and the deformation mechanism. Even more, when a polyethylene with high crystallinity, such as high-density polyethylene (HDPE), is subjected to uniaxial tensile stretching, an inhomogeneous deformation, i.e., a necking, usually occurs. To understand the process of the deformation, the true stress−true strain dependence must be determined. With the aid of a video-control focusing on the neck center, the true stress−true strain relationship was measured, and basic properties of the deformation mechanism during the uniaxial tensile drawing could be revealed.[11−13] Typically, various deformation characteristics can be found in the different deformation stages. In the initial stage, the response of polyethylene to the external force shows Hookean elasticity. Further increasing the stress yielding and strain softening show up, and the sample undergoes a large deformation. Finally, when the limitation in the extensibility of the amorphous network is reached, strain hardening is brought out.[8] On the basis of numerous observations, we introduced three critical points associated with (1) the onset of local flow processes at the end of the Hookean range (point A), (2) a collective onset of sliding processes of the crystal blocks composing the crystal lamellae, which determines the yield point (point B), and (3) the beginning of a disintegration of the crystal blocks which is followed by a fibril formation (point C). The structural changes have been followed in detail.[4,5,10] Before the onset of fibrillation, lamellae, being embedded in the amorphous matrix, endure shear yield mostly via a chain and block sliding. Chains at first get preferentially oriented 45° away from the deformation direction corresponding to the direction of the maximum resolved shear stress. When the stress transferred by the amorphous network is high enough, fibrillation sets in and the molecular orientation shifts toward the deformation direction. With the aid of step-cycle tests it was shown that point C is also associated with a saturation of the reversible strain.[12−14] For polyethylene the critical strain related to the onset of fibrillation is about 0.6, independent of the crystallinity and branch content. Stress relaxation measurements yielded a decomposition of the measured stress into the viscous part and the quasi-static contributions of the amorphous network and the crystalline skeleton. Some of us recently proposed a model treating tensile deformation of semicrystalline polymers, in which the drawing stress is considered as being composed of these three components, namely (i) the forces transmitted by the skeleton of crystal blocks, (ii) the force brought up by the stretched amorphous network, and (iii) viscous forces.[15,16]

So far, most of the work has been carried out for isotropic samples, in which lamellae with different orientations with respect to the deformation direction can undergo different deformation processes.[17,18] Lamellae with a surface normal parallel to the deformation direction adopt interlamellar separa-

* Corresponding authors. Qiang Fu: Fax +86 28 8540 5402; e-mail qiangfu@scu.edu.cn. Ke Hong: Fax +49 761 203 5855; e-mail hong@physik.uni-freiburg.de.

10.1021/ma052496g CCC: $33.50
Published on Web 03/07/2006

tion, whereas those with a normal oblique to the deformation direction endure interlamellar slide. For oriented samples, drawn from the melt, it is well established that molecular chains are oriented under stress and form a shish structure as primary nuclei, which then induces the transverse growth of lamellae. In this way the shish-kebab structure with the well-defined lamellar orientation can be obtained.[19−22] As the morphological structure determines the mechanical properties of materials, one may expect to observe a different tensile deformation behavior in stretching a preoriented sample. In this paper, we present such results on an oriented HDPE sample. Comparing it with the isotropic counterpart, we found that the oriented HDPE not only showed a higher modulus but also did not exhibit necking during the tensile deformation. Moreover, the true strain related to the onset of fibrillation was shifted down to 0.3. A main difference showed up in the stress relaxation experiments which indicated a much higher viscous force. In fact, the changes in the tensile deformation characteristics of HDPE resulting from a preorientation can mostly be ascribed to an enhanced viscous force.

2. Experimental Section

2.1. Materials and Sample Preparation. The high-density polyethylene with $M_n = 7.8 \times 10^5$, $M_w = 9.2 \times 10^5$, and $M_w/M_n = 11$ used in the study was produced by Daqing Petrochemical Corp., China. It has a melt flow index (MFI) of 0.3 g/10 min, a crystallinity $\phi_c = 0.61$, and a melting point of about 135 °C. Samples for the mechanical test were prepared by the procedure of the melt extrusion drawing to be described as follows. Tapes with a thickness of 1 mm were first extruded using a Haake counter-rotating twin-screw extruder with a barrel temperature of 160−200 °C, followed by a die drawing with the aid of rollers. After drawing, the thickness of the tapes was reduced to about 0.3 mm, corresponding to a drawing ratio of about 8 (as given by the change in the cross-sectional area). Specimens with dog-bone shape were punched from the oriented tapes along the original melt extrusion direction. The crystallinity of this oriented sample is 0.65, as determined by DSC.

2.2. Two-Dimensional Small-Angle X-ray Scattering. 2D SAXS measurements were carried out using an in-house setup with a rotating anode X-ray generator (Rigaku RU-H300, 18 kW) equipped with two parabolic multilayer mirrors (Bruker, Karlsruhe), giving a highly parallel beam (divergence about 0.012°) of monochromatic Cu Kα radiation ($\lambda = 0.154$ nm). The SAXS intensity was recorded with a two-dimensional gas-filled wire detector (Bruker Hi-Star). A semitransparent beamstop placed in front of the area detector allowed monitoring the intensity of the direct beam. The SAXS intensities were normalized to the intensity of the direct beam. Azimuthal scans of 2D SAXS were made with 1° steps.

2.3. Two-Dimensional Wide-Angle X-ray Scattering. 2D WAXS experiments were conducted using a Rigaku Denki RAD-B diffractometer. The wavelength of the monochromated X-ray from Cu Kα radiation was 0.154 nm, and the transmission mode was used. The in-situ stretching of the oriented samples was realized by employing a Mini-Instron (Rheometric Scientific Mini Mat2000), and thus samples could be kept under stress during the exposure.

2.4. True Stress−True Strain Measurement. According to the procedure developed by G'Sell,[23] true stress−strain curves were measured using an INSTRON 4301 machine equipped with a CCD camera which regulated the crosshead speed so that a constant local strain rate in the narrowest part of the specimen was maintained. Since the oriented HDPE samples can deform homogeneously, rather than with the aid of video-controlled measurements in the common cases, true stress−strain dependencies could be obtained without video control and therefore with a higher accuracy. The true stress (σ)−true strain (denoted ϵ_H, also known as Hencky strain) curve could be directly obtained assuming a constant volume relationship by

$$\sigma = \frac{F}{A} = \frac{F}{A_0}\lambda \tag{1}$$

(F is the load, A the varying sample cross section, A_0 the initial cross section, and λ the extension ratio) and

$$\epsilon_H = \ln \lambda \tag{2}$$

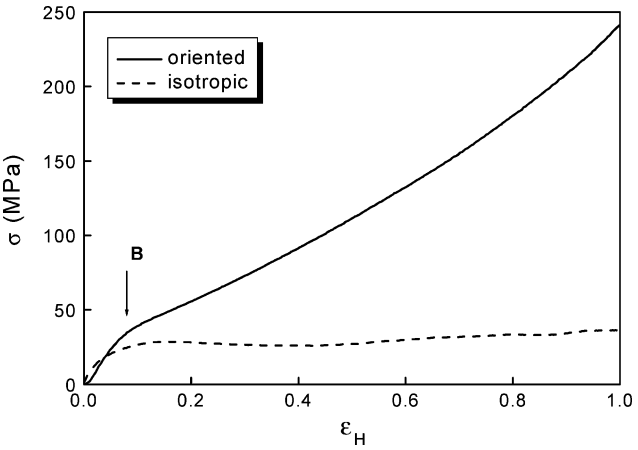

Figure 1. True stress−true strain dependencies obtained for an oriented and an isotropic sample of HDPE at a strain rate $d\epsilon_H/dt = 0.005\ s^{-1}$.

2.5. Step-Cycle Tests. Elastic properties in the deformed state could be derived from step-cycle tests. The sample was deformed step by step with a constant Hencky strain rate. After each step, the sample's strain rate was inverted and used to contract the sample until a stress of zero was reached. Thereafter, the sample was extended again until it re-reached the point at which it left the stretching curve. With the aid of step-cycle tests, the total true strain could be partitioned into a reversible (cyclic) and an irreversible (basic) part in a well-defined way.

2.6. Stress Relaxation Experiments. A test specimen was stretched first to a predetermined strain at a constant Hencky strain rate $d\epsilon_H/dt$. Subsequently, the strain was held constant and the force decay was followed with time. Stress relaxation measurements at constant strain provide a means to determine the viscous forces.

3. Results

3.1. Stretching Curve. Usually, formation of a neck with a load drop around the yield point is observed in the engineering stress−strain curve for isotropic polyethylene with a high crystallinity such as HDPE. For the oriented HDPE sample a load drop is found neither in the engineering nor in the true stress−strain curve. The stretching curve $\sigma(\epsilon_H)$ for a constant true strain rate of $0.005\ s^{-1}$ is shown in Figure 1, together with that of an isotropic sample for comparison. The shape of the curve indicates a strain softening which is later followed by a hardening. In engineering stress−strain curves the yield point for necking samples is associated with the stress maximum, while in nonnecking samples it is usually identified with the point on the curve where the curvature takes on the maximum value. The latter choice is also convenient for true stress−true strain curves of semicrystalline polymers where a stress maximum does not occur. We call the thus-determined yield point "point B". For the oriented sample we find, as indicated in Figure 1, $\epsilon_H(B) = 0.1$. Compared to the isotropic sample, the oriented HDPE has a much larger drawing stress and shows a stronger strain hardening.

Figure 2 presents the true stress−true strain curves for the oriented HDPE for various strain rates. All of the curves show

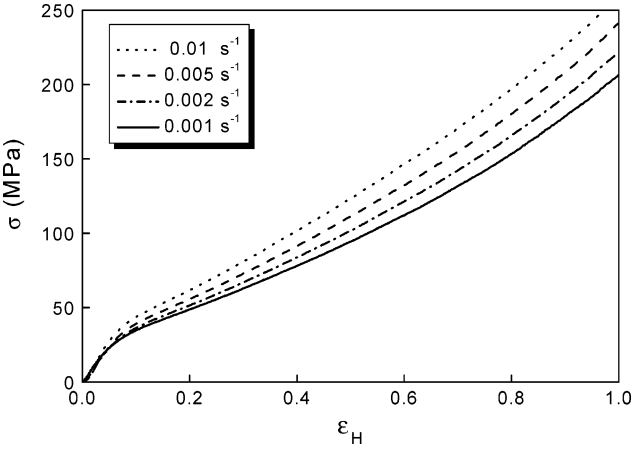

Figure 2. True stress−true strain dependencies obtained for oriented HDPE at the indicated strain rates.

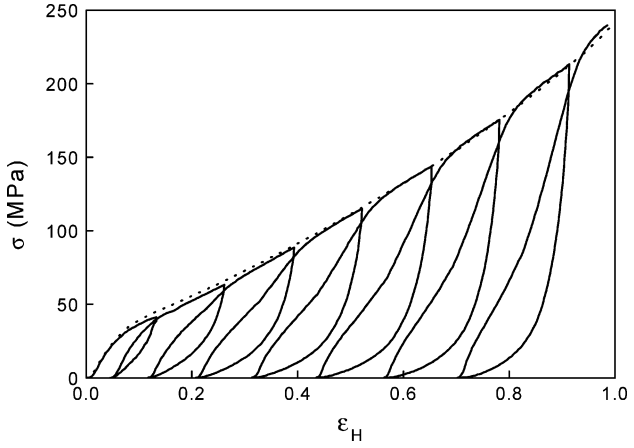

Figure 3. Oriented HDPE: step-cycle test carried out with a strain rate 0.005 s^{-1}. Comparison with the stretching curve of Figure 1 (broken line).

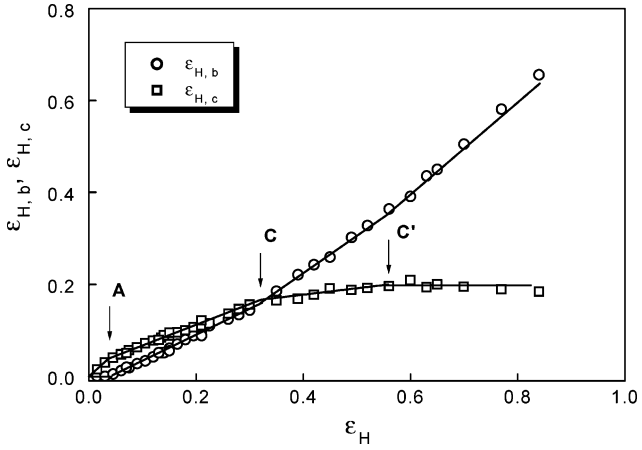

Figure 4. Oriented HDPE: Cyclic and basic part of the total strain as derived from step-cycle tests like the one shown in Figure 3.

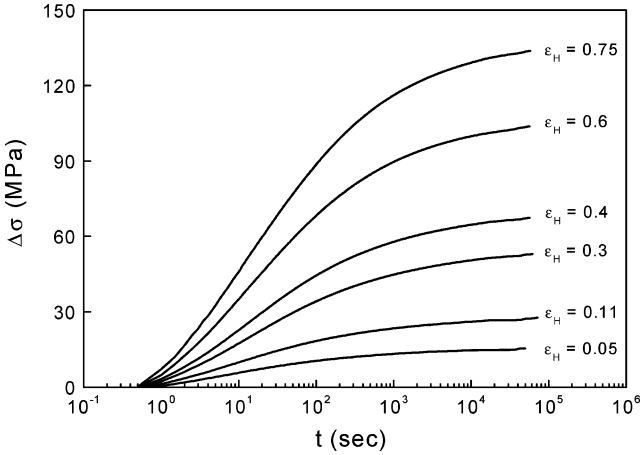

Figure 5. Oriented HDPE: the amount of the stress relaxation $\Delta\sigma(t) = \sigma(0) - \sigma(t)$ after a stretching with strain rate of 0.005 s^{-1} to the given initial strains.

a common shape. At point B a strain softening shows up, and at high deformation a hardening occurs. The result shows that application of a larger strain rate leads to a larger drawing stress when extending the sample.

3.2. Step-Cycle Test. Figure 3 presents the result of a step-cycle test for the oriented HDPE sample conducted with a strain rate of 0.005 s^{-1}. For a comparison, the continuous stretching curve is also included. It is found to agree with the series of steps. Hence, the interruption by the cycles does not change the stretching properties. The "cyclic strain" recovered in the unloading down to zero stress, $\epsilon_{H,c}$, gives the elastic part, and the remaining "basic strain", $\epsilon_{H,b}$, represents the irreversible plastic part in the time scale of this particular experiment rather than the permanent truly irreversible plastic strain, which is usually lower.[12] The results of this decomposition carried out at various total strains are presented in Figure 4.

An irreversible part of the strain exists already below the yield point as is shown by Figure 4. In fact, plastic flow sets in already at the very beginning of the stretching and shows a break at a strain $\epsilon_H = 0.04$ where we allocate the critical point A. As shown by Figure 4, around $\epsilon_H = 0.3$, a break occurs in the development of the cyclic part, from the previous linear increase to a decreased slope. Here, we allocate the critical point C. A maximum value is then reached at point C′ (strain $\epsilon_H = 0.55$). From this strain upward, further extension is exclusively due to an increase of the irreversible component.

3.3. Stress Relaxation Measurements. Stress relaxation measurements at a constant strain provide a means to determine the viscous forces. Figure 5 presents the time-dependent function of the true stress decay, $\Delta\sigma(t) = \sigma(0) - \sigma(t)$, for oriented HDPE. One finds that after a short initial period the decay obeys a logarithmic law, $\Delta\sigma \sim \log t$. This range is finite; finally, the stress approaches a quasi-stationary state. We set the maximum time of the experiment to 10 h. The remaining stress can be considered as quasi-stationary; the viscous force is to be identified with the total amount of stress decay, $\Delta\sigma(t = 36000$ s). Figure 6 shows the result of the decomposition of the stretching curve $\sigma(t)$ into a viscous and a quasi-stationary part. Both the viscous and the quasi-static stress are enhanced with increasing strain, with a faster rate for the viscous stress and a lower rate for the quasi-static stress. Interestingly, the figure shows clearly that the viscous stress dominates the total drawing stress. Especially at high strains, the viscous stress takes up more than 70% of the total stress.

3.4. Structure Evolution. The initial oriented texture obtained in the melt extrusion drawing shows up in both 2D SAXS and 2D WAXS patterns, as given in Figure 7. Evidently, the SAXS scattering maxima are on the meridian, i.e., the melt extrusion direction, indicating that an oriented texture is formed with the normal of lamellae parallel to the melt extrusion direction. During melt drawing, HDPE forms at first many shish fibers, which in turn serve as primary nuclei for the growth of the kebab lamellae. The transverse growth of each kebab is constrained by the neighbor shish-kebabs.[26,27] The narrow space between two neighbor shish-kebabs which resemble cylinders shows up in the SAXS pattern in the streak along the equator. Consistent

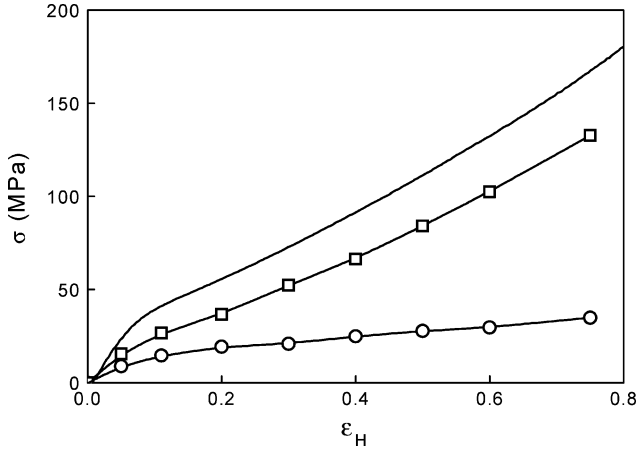

Figure 6. Oriented HDPE: stress−strain curves for strain rate of 0.005 s^{-1}, amounts of stress decay $\Delta\sigma$ various fixed strains after a relaxation time of 36000 s (open squares), and quasi-static stress−strain dependence as obtained by subtraction of $\Delta\sigma$ from the drawing stress (open circles).

with the results of 2D SAXS, the (110) and (200) lattice planes, concentrated at the equator in 2D WAXD pattern, indicate that chains are oriented parallel to the melt extrusion drawing direction. The intensity maximum of a (110) plane at the equator suggests the existence of a fiber structure in the sample. The results of 2D SAXS and 2D WAXS demonstrate that the sample has a high lamellar and chain orientation.

Changes in the orientation of HDPE during stretching can be observed by the in-situ registration of 2D WAXS patterns. Figure 8 gives azimuthal scans of the (110), (200), and the halo intensity of the oriented sample at different strains. The intensity scale in this figure represents an integral peak intensity.The intensity plots of amorphous halo is constructed just by simple measurement of the intensity at the $2\theta = 19.5°$, which is the expected position of maximum of amorphous halo. These data may include some unwanted contribution from the shoulder of the very intense (110) Peak. Since the data were collected on sample under the same experiment condition just different strains, the systematic error can be neglected thus a relative comparison is possible.

Before stretching, the (110) reflection shows a maximum at the equator with two small shoulders. When drawing the sample, the two shoulders weaken and finally disappear. This change indicates that all crystallites transform into fibers. With increasing strain, the thickness of the sample becomes thinner, which leads to a lower scattering intensity. Therefore, it is not surprising that in Figure 8 the intensity of the peak located at the equator decreases on increasing the strain. After correcting the thinning effects, the intensity of the peak shows an increase when the strain goes to a large value.

4. Discussion

4.1. Viscous Force. The relaxation measurements show that after a finite range wherein the decay follows a logarithmic law a quasi-stationary state is reached. By subtracting the quasi-static stress from the total stress, the viscous stress is obtained, and the result is shown in Figure 6. The viscous stress accounts globally for all viscous forces which originate from motions within both the crystalline and the amorphous regions. It is astonishingly large if compared to the isotropic samples. Obviously, the much enhanced viscous force is to be related to the oriented structure. Shish-kebabs, i.e., stacks of lamellae interconnected by a central fiber, are the characteristic elements in polyolefin samples prepared via melt extrusion drawing. It can be expected that the presence of shish-kebabs enhances the interlamellar coupling.[11] Since the deformation of polyolefins is related to the gradual destruction of the interlamellar order, an enhanced interlamellar coupling will result in a higher resistance to the deformation, i.e., in a higher viscous force. Other examples for an enhancement of the viscous force by the orientation following from an extrusion drawing are isotactic polypropylene (i-PP) and linear low-density polyethylene (LLDPE), as is shown in Figure 9. For an oriented i-PP with a crystallinity of $\phi_c = 0.48$, the viscous stress is again the dominant part in the stretching stress; for an oriented sample of LLDPE the viscous stress is still comparable to the quasi-static stress. Other two possibilities should be also considered to understand the observed high viscous force. (1) Since nearly all lamellae are oriented with chain direction along the stretch the resolved shear stress for crystallographic chain slip is very low, therefore higher stresses are required to activate deformation of crystals by crystallographic mechanisms. This can explain the observation of higher viscous stress in materials of higher crystallinity (HDPE > iPP > LLDPE, see Figure 9). (2) The influence of the resultant specific morphology of oriented sample should be also considered. Such structure should modify markedly the viscous force and hence the overall mechanical response. For example, the interlocking of kebabs was observed and has been associated with the high modulus of PE by Bahir and Odell.[28]

The effective modulus as derived from the initial slopes of the stretching curve in Figure 6 includes both the viscous stress and the true elasticity.[16] It is interesting to note that the enhancement of the modulus of the oriented compared to the isotropic sample mainly originates from the increase of the viscous force. For example, the effective modulus of 500 MPa of the oriented HDPE is set up of 320 MPa originating from a linearly increasing viscous force and 180 MPa coming from the quasi-static stress. The result shows that the higher effective modulus observed for the oriented sample is not primarily due to the fibers, i.e., the shish in the structure, but mostly due to the viscous forces between the shish-kebabs which arise during deformation. Note that the modulus of 500 MPa for oriented HDPE is rather low; this may result from a low degree of orientation of the sample obtained via melt extrusion drawing, compared to that as obtained via spinning.

4.2. Strain Dependence of the Reference Stress. A recently introduced model describes the stress which has to be brought up when stretching a semicrystalline polymer sample as is indicated in Figure 10.[15] It is set up by three branches associated with a viscous force, σ_r, the rubber-elastic force of the entanglement network, σ_n, and the force transmitted by the skeleton of crystallites, σ_c. As one application, the model can be used to deal with the stress relaxation. The kinetics of stress relaxation relates to the upper branch, σ_r, only. Besides an elastic element, with modulus E_r, it incorporates a dashpot representing the viscosity and assumes for the latter validity of the Eyring equation

$$\frac{\sigma_r}{\sigma_0} = \mathrm{asinh}\left(\frac{\dot{\epsilon}_H}{\dot{\epsilon}_0}\right) \tag{3}$$

It includes two parameters: the reference stress σ_0 and the reference strain rate $\dot{\epsilon}_0$.Therefore, the kinetics of the stress

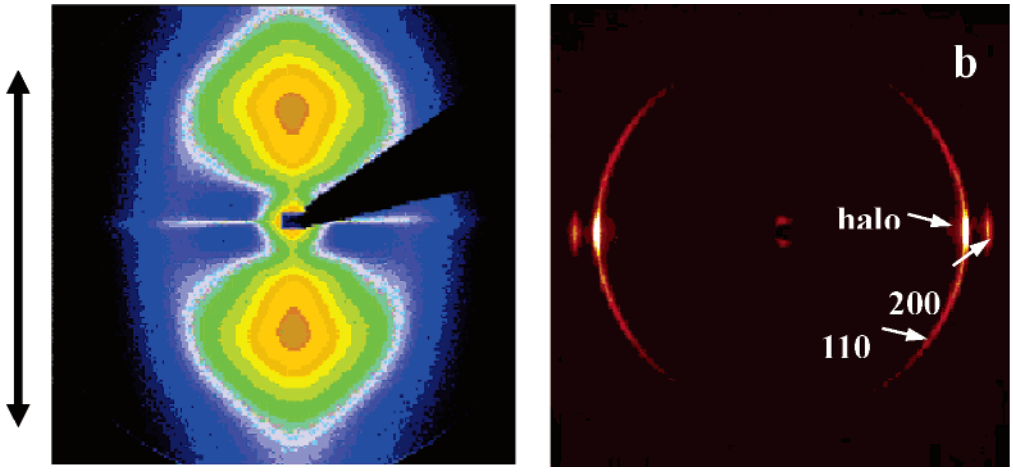

Figure 7. Oriented HDPE: scattering patterns of 2D SAXS (a) and 2D WAXS (b). The extrusion direction is noted in this figure.

relaxation can be determined by the following differential equation

$$\dot{\epsilon}_H = \frac{\dot{\sigma}_r}{E_r} + \dot{\epsilon}_0 \sinh\left(\frac{\sigma_r}{\sigma_0}\right) = 0 \tag{4}$$

or

$$\frac{d}{dt}\frac{\sigma_r}{\sigma_0} = -\frac{1}{\tau_r}\sinh\left(\frac{\sigma_r}{\sigma_0}\right) \tag{5}$$

with

$$\tau_r^{-1} = \frac{\dot{\epsilon}_0 E_r}{\sigma_0} = \frac{E_r}{\eta_0} \tag{6}$$

Here, τ_r denotes the relaxation time which would be found in the Newtonian limit of very low stress σ_r, and η_0 is the viscosity coefficient. Equation 5 is solved by the expression

$$\Delta\sigma = \sigma_r(0) - 2\sigma_0 \operatorname{atanh}\left[\tanh\left(\frac{\sigma_r(0)}{2\sigma_0}\right)\exp\left(-\frac{t}{\tau_r}\right)\right] \tag{7}$$

It follows that σ_0 can be either derived from the slope of the $\Delta\sigma$ vs log t curve or from the strain rate dependence of σ according to eq 3, which can be approximated by

$$\sigma_r \approx \sigma_0 \ln\left(\frac{\dot{\epsilon}_H}{\dot{\epsilon}_0}\right) \tag{8}$$

Figure 11 presents the reference stress as a function of the imposed strain as it follows from the slope in the logarithmic decay time range. The reference stress increases with rising strain. The values of σ_0 are large compared to those found for an isotropic sample,[15] again expressing that the investigated oriented sample has a much larger viscous stress.

Figure 2 showed that the drawing stresses increase with increasing strain rate. The dependence of the drawing stress on the strain rate for strains of 0.2, 0.4, and 0.6 is shown in Figure 12. It obeys the Eyring equation. The reference stress σ_0 thus can be extracted for linear fits, and the values obtained are $\sigma_0(\epsilon_H = 0.2) = 5.3$ MPa, $\sigma_0(\epsilon_H = 0.4) = 10.2$ MPa, and $\sigma_0(\epsilon_H = 0.6) = 14.6$ MPa. They perfectly agree with the results derived from the stress relaxation measurements given in Figure 11. The agreement validates the model, which splits the total stress in a strain rate dependent viscous part and a quasi-static, i.e., strain rate independent part.

4.3. Necking vs Homogeneous Deformation during Tensile Deformation. When an isotropic polyethylene with high crystallinity such as HDPE is subjected to the tensile deformation, necking always occurs. The neck formation leads to a decrease of the load. In our case of an oriented HDPE, the sample can be deformed homogeneously; no necking occurs. On the basis of a measurement of the true stress−true strain dependence, one can always estimate whether the material shows necking during a tensile deformation.[29] If we choose the data of Figure 1 and divide the true stresses by $\exp(\epsilon_H)$, the nominal stress is obtained (assuming volume constancy). In Figure 13 the result is plotted vs the true strain. For the isotropic HDPE the curve shows a maximum at $\epsilon_H \approx 0.1$. This maximum indicates occurrence of a mechanical instability, i.e., necking formation. A different result follows for the oriented HDPE. There is no load maximum and hence no necking. Necking is a very interesting phenomenon and has been widely investigated. The concept proposed here is based on the same true strain related to lamellar fragmentation and has some limitations to apply for the large strain deformation.Necking under tensile stretching can be interpreted with Considere's construction. The ratio of σ_y/G has a critical value of 3, practically above which the Considere's principle for necking is satisfied, where σ_y is the intrinsic yield stress, G is the strain hardening modulus, and λ is the draw ratio.

The reason for the difference is the steeper increase of the true stress in the oriented sample, and this steeper increase is primarily due to the much enhanced viscous force. Since the glass transition of polyethylene is far below the test temperature, it mainly depends on the forces accompanying the plastic deformation of the crystallites whether or not necking occurs. For the oriented sample the stress softening at the yield point is reduced and leads no longer to a load drop. One may ask about the origin of the large viscous stress. It is the presence of the shish-kebabs which leads to the existence of a zipperlike structure of stacked lamellae. This zipperlike structure enhances the forces acting against the sliding and thus produces a high viscosity.

4.4. True Strains Related to the Onset of Fibrillation. Tensile deformation mechanisms change at several critical points.[12,13,24,25] Here we address point C, the beginning of a disintegration of the crystal blocks and the onset of fibrillation. At point C the extended network has reached the critical stress which is necessary to destroy the crystal blocks. For a certain polymer a one-to-one relationship exists between the network

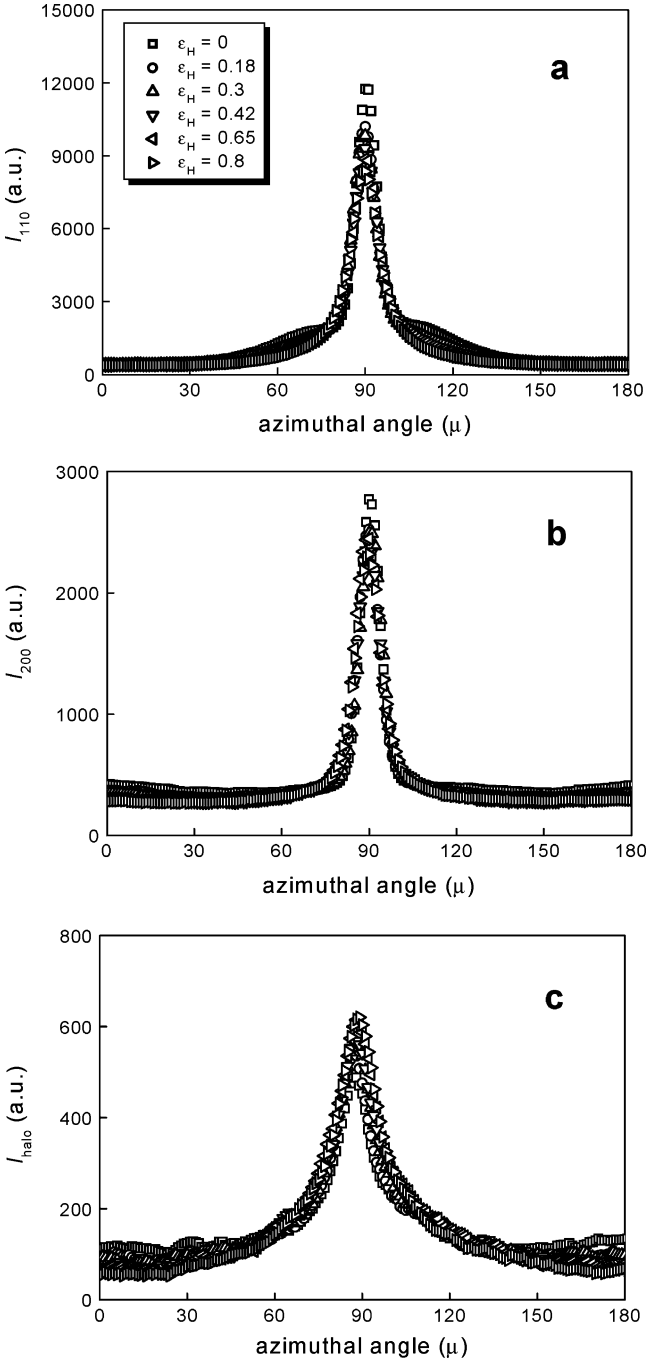

Figure 8. Oriented HDPE: azimuthal intensity distribution of the (110) (a), (200) reflections (b), and of the amorphous halo (c), measured at the indicated imposed strains.

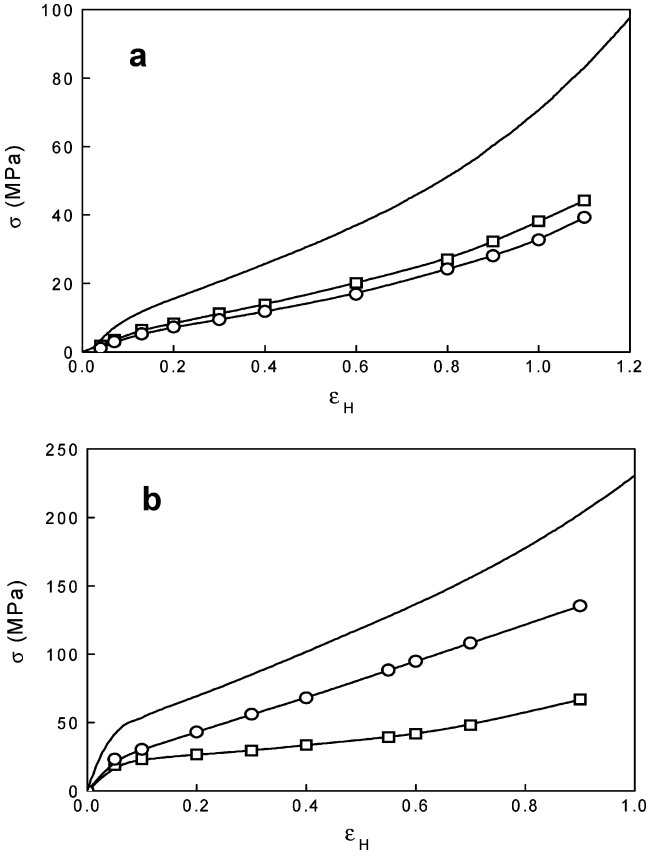

Figure 9. Oriented LLDPE (a) and oriented i-PP (b): stress−strain curves for strain rate of 0.005 s^{-1}, relaxed stresses measured at various fixed strains after a relaxation time of 36000 s (open squares), and quasi-static stress−strain dependence as obtained by subtraction the relaxed stress from the drawing stress (open circles).

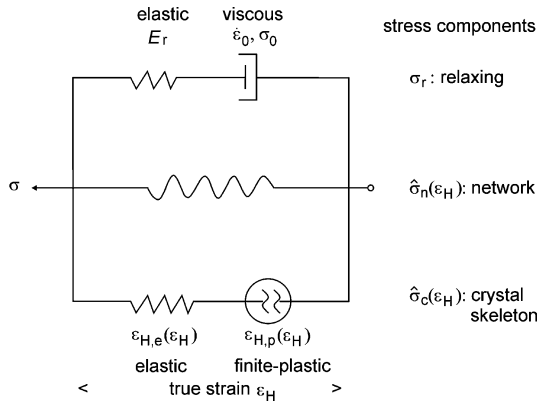

Figure 10. A three-component model treating the tensile deformation properties of semicrystalline polymers.

stress and the degree of orientation of the amorphous chain sequences.

The degree of orientation can be determined by measuring the azimuthal intensity distribution of the amorphous halo.[30] An orientational order parameter proposed by Hermanns is used to express for uniaxially oriented samples the degree of orientation related with both a set of lattice planes (*hkl*) or the chain sequence packing reflected in the amorphous halo.[31] It is defined by

$$S = (3\langle\cos^2 \vartheta\rangle - 1)/2 \tag{9}$$

Here ϑ denotes the angle between the stretching direction and the normal vector onto the lattice plane or onto the amorphous chain sequence. The value of the order parameter can be derived from the azimuthal intensity distribution function $I(\mu)$ along the respective circle by using the Polanyi equation[32]

$$\cos^2 \vartheta = \cos \theta \cos \mu \tag{10}$$

The equation relates the azimuthal angle μ along the Debye circle to the angle ϑ between the stretching direction and the normal vector.

The results for the orientational order parameters of the (110) and (200) reflections and the amorphous halo are given in Figure 14 as a function of the imposed strain. Note that, for a perfect orientation when the normal is in the plane of equator, the orientational order parameter would be $S = -0.5$. This limiting value was not reached.

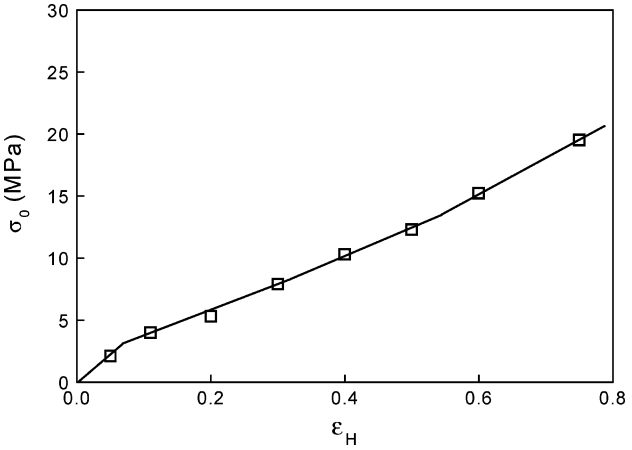

Figure 11. Oriented HDPE: variation of the reference stress σ_0 with the imposed strain as derived from the slopes of the stress relaxation curves in Figure 5.

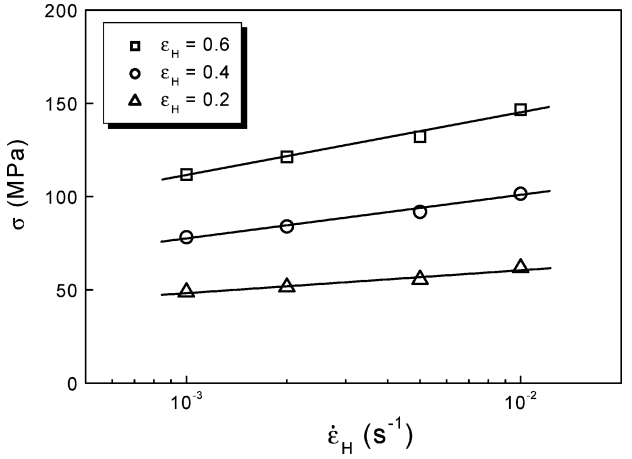

Figure 12. Oriented HDPE: drawing stress as a function of the strain rate at the indicated strains. Data are from Figure 2.

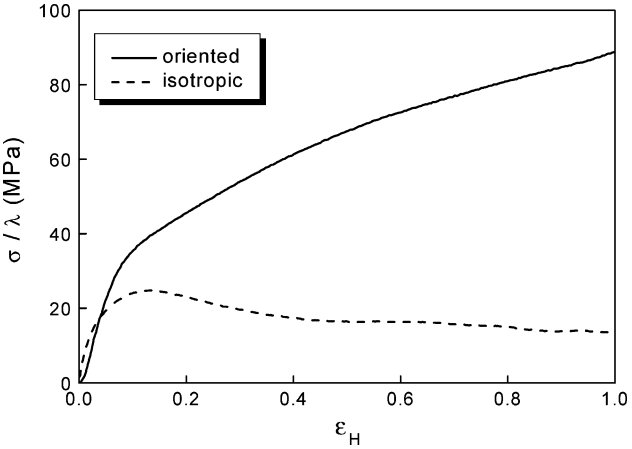

Figure 13. Dependencies between σ/λ and ϵ_H for oriented and isotropic HDPEs.

The results show that the crystallites as well as the amorphous sequences are oriented from the beginning. On imposing the strain the orientation further increases. The order parameter of the halo has a break at $\epsilon_H = 0.3$, at a value of the orientational order parameter of about -0.2. For isotropic polyethylenes, the beginning of disintegration of the crystal blocks and onset of fibrillation (point C) is located at around $\epsilon_H = 0.6$. For the oriented sample the fibrillation sets in earlier. The reason is obvious: The amorphous network of the oriented HDPE is already stretched in the initial state, and the network stress then

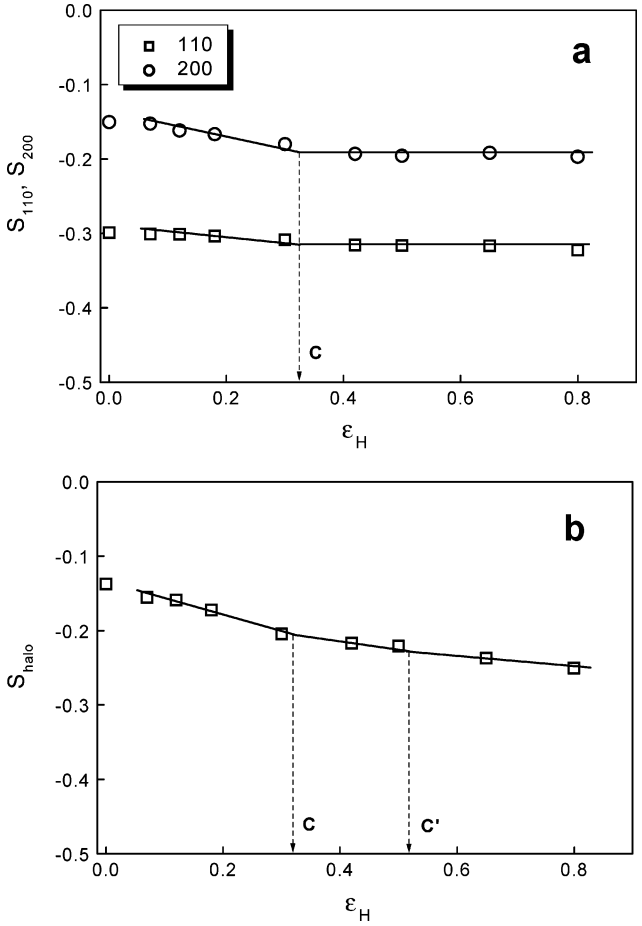

Figure 14. Oriented HDPE: orientational order parameters associated with the (110) and (200) reflections and the amorphous halo as a function of the imposed strains.

reaches the critical value necessary to destroy the crystal blocks earlier. $S_{halo}(\epsilon_H = 0.3) = -0.2$ for oriented HDPE is comparable to the value of S_{halo} at point C for isotropic PE.[30] For this reason we assign for the oriented sample point C to $\epsilon_H = 0.3$. In a recent publication Bartczak et al. suggested that the point C corresponds to the extensibility limit of the amorphous network due to that the full extension of tie molecules is reached.[33−35] Here our result is in line with their hypothesis of origin of point C; that is, initially oriented amorphous material must have the limiting stretch lower than the isotropic sample. This difference should result in the shift of point C to lower strain. It should be also noted that the point C should be related to the orientation parameter. The higher the degree of orientation, a shift to lower value is expected.

5. Conclusion

Mechanical tests under an uniaxial tensile deformation have been conducted for an oriented HDPE sample obtained via melt extrusion drawing. No necking occurs in these samples. Relaxation properties have been studied with the aid of step-cycle tests. The true strain at the onset of fibrillation is about 0.3, at the same degree of orientation of the amorphous chain as in isotropic samples, as deduced from the azimuthal intensity distribution of the halo. The main finding is a strong enhancement of the viscous forces compared to isotropic PEs. As determined by stress relaxation measurements, the viscous force takes up 70% of the total stress. The presence of shish-kebabs interconnecting neighbor lamellae in the stack seems to be the reason for the high viscous force.

Acknowledgment. We express our great thanks to the National Natural Science Foundation of China (50533050, 50373030, and 20490220) for financial support. Support of this work by the Deutsche Forschungsgemeinschaft (Sonderforschungsbereich 428) is gratefully acknowledged.

References and Notes

(1) Zhou, H. Y.; Wilkes, G. L. *Polymer* **1998**, *39*, 3597.
(2) Bartczak, Z.; Argon, A. S.; Cohen, R. E. *Polymer* **1994**, *35*, 3427.
(3) Seguela, R.; Elkoun, S.; Gaucher-Miri, V. *J. Mater. Sci.* **1998**, *33*, 1801.
(4) Butler, M. F.; Donald, A. M.; Ryan, A. J. *Polymer* **1997**, *38*, 5521.
(5) Butler, M. F.; Donald, A. M. *Macromolecules* **1998**, *31*, 6234.
(6) GaucherMiri, V.; Seguela, R. *Macromolecules* **1997**, *30*, 1158.
(7) Butler, M. F.; Donald, A. M.; Bras, W.; Mant, G. R.; Derbyshire, G. E.; Ryan, A. J. *Macromolecules* **1995**, *28*, 6383.
(8) Haward, R. N. *Macromolecules* **1993**, *26*, 5860.
(9) Pazur, R. J.; Ajji, A.; Prudhomme, R. E. *Polymer* **1993**, *34*, 4004.
(10) Bartczak, Z.; Galeski, A. *Polymer* **1999**, *40*, 3677.
(11) G'Sell, C.; Joas, J. J. *J. Mater. Sci.* **1979**, *14*, 583.
(12) Hiss, R.; Hobeika, S.; Lynn, C.; Strobl, G. *Macromolecules* **1999**, *32*, 4390.
(13) Hobeika, S.; Men, Y.; Strobl, G. *Macromolecules* **2000**, *33*, 1827.
(14) Al-Hussein, M.; Strobl, G. *Macromolecules* **2002**, *35*, 8515.
(15) Hong, K.; Rastogi, A.; Strobl, G. *Macromolecules* **2004**, *37*, 10165.
(16) Hong, K.; Rastogi, A.; Strobl, G. *Macromolecules* **2004**, *37*, 10174.
(17) Keller, A.; Pope, D. P. *J. Mater. Sci.* **1971**, *6*, 453.
(18) Pope, D. P.; Keller, A. *J. Polym. Sci., Polym Phys. Ed.* **1975**, *13*, 533.
(19) Eder, G.; Janeschitz-Kriegl, H.; Liedauer, S. *Prog. Polym. Sci.* **1990**, *15*, 629.
(20) Okamoto, M.; Kubo, H.; Kotaka, T. *Macromolecules* **1998,** *31*, 4223.
(21) Kumaraswamy, G.; Issaian, A. M.; Kornfield, J. A. *Macromolecules* **1999**, *32*, 7537.
(22) Somani, R. H.; Hsiao, S.; Yang, L. *Macromolecules* **2002**, *35*, 9096.
(23) G'Sell, C.; Hiver, J. M.; Dahoun, A.; Souahl, A. *J. Mater. Sci.* **1992**, *27*, 5031.
(24) Men, Y.; Strobl, G. *J. Macromol. Sci., Phys.* **2001**, *B40*, 775.
(25) Men, Y.; Strobl, G. *Macromolecules* **2003**, *36*, 1889.
(26) Keller, A. *Polymer* **1962**, *3*, 293.
(27) Schrauwen, B. A. G.; Breemen, L. C. A. v.; Spoelstra, A. B.; Govaert, L. E.; Peters, G. W. M.; Meijer, H. E. H. *Macromolecules* **2004**, *37*, 8618.
(28) Bashir, Z.; Odell, J. A. *J. Mater. Sci.* **1993**, *28*, 1081.
(29) Strobl, G. *The Physics of Polymers;* Springer: Berlin, 1996; p 357.
(30) Hong, K.; Strobl, G. *Macromolecules*, in press.
(31) Hermanns, P. H.; Platzek, P. *Kolloid Z.* **1939**, *88*, 68.
(32) Polanyi, M. *Z. Phys.* **1921**, *7*, 149.
(33) Bartczak, Z. *Polymer* **2005**, *46*, 10339.
(34) Bartczak, Z.; Lezak, E. *Polymer* **2005**, *46*, 6050.
(35) Bartczak, Z.; Kozanecki, M. *Polymer* **2005**, *46*, 8210.

MA052496G